Enhancement of a whispering gallery mode microtoroid resonator by plasmonic triangular gold nanoprism for label-free biosensor applications

H. Nadgaran and M. Afkhami Garaei

Citation: J. Appl. Phys. **118**, 043101 (2015); doi: 10.1063/1.4927266
View online: http://dx.doi.org/10.1063/1.4927266
View Table of Contents: http://aip.scitation.org/toc/jap/118/4
Published by the American Institute of Physics

JOURNAL OF APPLIED PHYSICS **118**, 043101 (2015)

Enhancement of a whispering gallery mode microtoroid resonator by plasmonic triangular gold nanoprism for label-free biosensor applications

H. Nadgaran[a] and M. Afkhami Garaei
Department of Physics, College of Science, Shiraz University, Shiraz 71454, Iran

(Received 12 October 2014; accepted 9 July 2015; published online 22 July 2015)

Whispering gallery mode microresonators coupled to plasmonic nanoparticles have shown great promise for ultra-sensitive and label-free biological sensing. We analyze a whispering gallery mode microtoroid biosensor with a triangular gold nanoprism bound to its surface. We choose triangular nanoprism because of its capability of considerable enhancement of electromagnetic field at the tips and because its localized surface plasmon resonance band position is readily tunable. The local electric field enhancement at different points of plasmonic triangular gold nanoprism is calculated and the effect of rounded tip is investigated. This field enhancement permits the detection and characterization of some large protein molecules. We have studied the detection of single bovine serum albumin protein using our hybrid microcavity. © *2015 AIP Publishing LLC*.
[http://dx.doi.org/10.1063/1.4927266]

I. INTRODUCTION

Nowadays, one of the most important applications of photonics is optical biosensors. Optical biosensors have been developed for fast and early detection of contaminants,[1,2] pathogen bacteria,[3] and drugs.[4] Perhaps, the most important factor in the sensitivity of these sensors is the number of light visit with the analyte molecule; this number is only once for most conventional waveguide-based sensors but can be several thousand times for resonator-based sensors[5] in which light returns in phase after each round trip. So in recent decades, biosensors based on optical resonators received considerable attention in ultrasensitive and label-free biosensing.[6] Whispering gallery mode resonators (WGMRs) are good candidates for acquiring high number of round trips leading to detection of individual bio-nanoparticles (NPs).[7,8] Vollmer *et al.*[9] report a label-free single virus detection by a WGMR for Influenza A (with a mass of 520 ag). Based on reactive sensing principle (RSP),[10] in order to enhance the resonance frequency shift, the electric field at the position of the particle should be increased, that is,

$$\frac{\Delta\omega_r}{\omega_r} = -\frac{\Delta\lambda_r}{\lambda_r} = -\frac{|W_p|}{W_c} \cong -\frac{\alpha_{ex}|E_0(r_v)|^2}{2\int \varepsilon_c |E_0(r)|^2 dV}, \quad (1)$$

where $E_0(r_v)$ and $E_0(r)$ are field amplitudes of the mode at the position of the nanoparticle (r_v) and in mode r, α_{ex} is the excess polarizability of the nanoparticles, and ε_c is the permittivity of the cavity.

The presence of plasmonic nanoparticles near the microresonator leads to locally enhance the evanescent field with degradation of Q-factor.[11] Reactive resonance shifts in WGMRs have been extensively studied in the literature together with perturbation of WGMR sensors from both dielectric and plasmonic nanoparticles perspective.[12–15]

Shopova *et al.*[16] demonstrated the interaction of target molecules in an equatorial carousel orbit with a plasmonic nanoparticle bound at the microresonator's equator. As the target molecule parks to hot spots on the plasmonic particle, frequency shifts were enhanced by a factor of four. Dantham *et al.*[17] report the label-free detection by a microsphere-plasmonic nanoshell hybrid resonator of the smallest RNA virus, MS2 with mass of only 1% of Influenza A (6 ag vs. 520 ag). Furthermore, the effect of shell thickness on electric field enhancement was calculated. As the shell thickness becomes small, the hot spots play an important role in the field intensity enhancement. Dantham *et al.*[18] have also demonstrated detection and characterization of the single thyroid cancer marker (Thyroglobulin, Tg) and bovine serum albumin (BSA) proteins (with masses of only 1 ag and 0.11 ag) using gold nanoshell receptor with intrinsic "random bumps." The overlap between short-range reactive fields and a single protein adsorbing to a bump leads to considerable increase in sensitivity compared to smooth shell. Moreover, some other plasmonic structures, such as nanorods and nanoellipsoids, were also investigated for the purpose of enhancement of the detection sensitivity of WGMRs.[19–22]

Anisotropic NPs with non-spherical structures (e.g., prisms, cubes) with unique shape-dependent properties and functionalities were also employed in a number of important applications to sensing.[23] Among these, triangular gold (TG) structure with sharp corners has attracted extensive interest because of their capability of considerable enhancement of electromagnetic field at the vertices. Similar to nanoshells and nanorods, the localized surface plasmon resonance (LSPR) band position of triangular gold nanoprisms is readily tunable from visible to IR by varying the tip sharpness, the edge length, and the aspect ratio (AR) (lateral dimension/thickness).[24] Additionally, sharper geometrical features also exhibit much stronger near field enhancements than that of nanoshells and nanorods.

The aim of this work is to study a triangular structure subject to WGMR evanescent field and investigate the effect

[a]Author to whom correspondence should be addressed. Electronic mail: nadgaran@susc.ac.ir

of the tip sharpness on the enhancement of the local electric field and on Q-factor.

A. Local field intensity enhancement factor (LFIEF)

LFIEF is defined to be the intensity of the electromagnetic field with respect to the intensity we would have had at the place without the plasmonic nanoparticle. The local field intensity at a specific point is proportional to the square of the electric field amplitude at that point, $|\boldsymbol{E}(\mathbf{r})|^2$. The LFIEF at a specific point is then the normalized value of $|\boldsymbol{E}(\mathbf{r})|^2$ with respect to the intensity of the incoming field at the point $|\boldsymbol{E}_0(\mathbf{r})|^2$. Explictly,[25]

$$LFIEF = \frac{|\boldsymbol{E}(\mathbf{r})|^2}{|\boldsymbol{E}_0(\mathbf{r})|^2}. \quad (2)$$

This dimensionless quantity can be >1 (enhanced) or <1 (quenched).

II. SIMULATION PROCEDURE

In this paper, the silica microtoroid is considered because of their ultra-high Q and ultra-small mode volume. The highest Q-factor recorded in a microtoroid is in excess of 1×10^8.[26] Unlike the complete theory developed for microspheres,[27] analytical expressions for the microtoroid mode structure are complicated and cannot be easily found. The optical mode for axially symmetric resonators[28] and non-axially symmetric resonators (when a WGM microtoroid resonator coupling to a nanoparticle) is usually calculated using a finite element method (FEM).[29,30] Our approach is similar to that proposed by Kaplan *et al.*[29] for a microtoroid geometry and discussed more fully in the work of Baaske *et al.*[22] For an unperturbed WGMR, a number of observations allow the simulation domain to be reduced to a toroid slice. Firstly, simulation of the full 2π range of the azimuthal angle is not required because a strong degree of azimuthal symmetry about the polar axis is present, thus usually the volume corresponding to $1/m$ of the original microtoroid is sufficient (m is the angular momentum component of the field due to the azimuthal symmetry $\exp[im\varphi]$). Secondly, the evanescent field penetrates only a short distance into the host medium, such that only a small region of the exterior needs be considered. Using this set of simplifications, the simulation domain can be reduced from a full toroid volume to that of a toroid slice as shown in Fig. 1. The side boundaries of the toroid got to be a reflector in order to represent that this section is part of a ring; we use the perfect magnetic conductor (PMC) boundary and as shown in Fig. 1(a), the electric field amplitude is maximum at the sides. The other boundaries can be set as open or as an absorber. The boundary conditions at the connection points of the slices are taken to be perfect reflectors; at the water-microtoroid boundary, the continuity of boundary conditions is implemented and the whole structure is bounded by a perfectly matched layer (PML) boundary conditions. Presence of the PML, moreover, allows the Q factor of each eigenmode to be extracted. A three-dimensional mode of this section is then computed with FEM to approximate the microtoroid fields and other parameters. In the presence of the nanoparticle that breaks the azimuthal symmetry, the angular slice must be wide enough to ensure that the nanoparticle has negligible effect at the boundaries. A variable mesh density is needed in our simulation since the field changes over different scales at different regions of the simulation. By mesh convergence analysis, decreasing the mesh size has been performed several times in order to find the optimal mesh size that does not change the results by less than 5%. Finer meshes were used in the vicinity of NP to allow greater spatial resolution in the resulting fields. Adding a small subdomain around the plasmonic particle can facilitate the increase in the mesh required. Also when studying WGMs supported within a microtoroid, the majority of the mode energy is concentrated near the outer surface of the microtoroid and is confined to lie in (or near) the equatorial plane of the microtoroid such that the centermost region of the microtoroid interior is of little interest and therefore by adding a small subdomain near the outer surface, we can

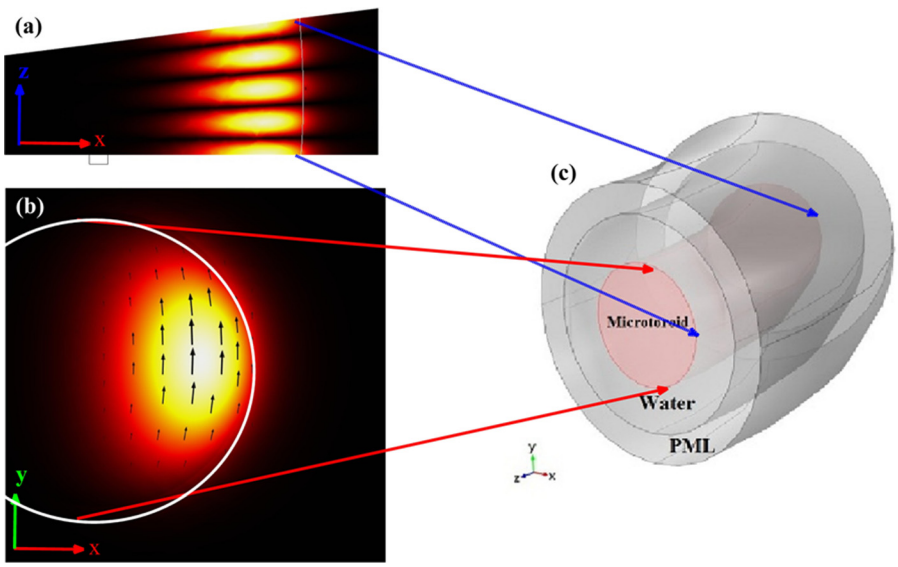

FIG. 1. Equatorial (x, z) (a) and polar (x, y) (b) cross-sections of the intensity distributions of WGMR for **TE** mode. Schematic of a toroid slice (c), simulation volume showing the division into distinct domains for the microtoroid, host medium, and PML.

facilitate the increase in the mesh require. Given these observations, the memory and time required to execute the simulation considerably can be reduced.

III. RESULTS AND DISCUSSIONS

Here, numerical calculations were performed to calculate the LFIEF of a hybrid microtoroid-TG nanoprism. In all computations, the toroid's principal and minor diameters were taken $\{D, d\} = \{36\,\mu\text{m}, 4\,\mu\text{m}\}$, respectively. The silica dielectric is assumed to be totally isotropic with relative permittivity of $\varepsilon_{\text{silica}} = 2.090$, corresponding to a refractive index of $n_{silica} = \sqrt{\varepsilon_{\text{silica}}} = 1.4457$. The **TM** and **TE** WGM resonance modes considered here (without the presence of nanoparticle) to occur at wavelengths of 1492.9 nm and 1499.9 nm, respectively, with WGM mode number of $m \cong 120$. We considered an isosceles triangular nanoprism immersed in the evanescent wave of the WGMR. The TG is much smaller than the microtoroid, and is illuminated by the field extending from the surface of the microtoroid. Gold refractive index is based on data from Palik[31] and the surrounding medium is assumed to be water with refractive index of n = 1.33. A conventional triangular prism consists of two triangles and three rectangles, where the triangles are the bases of the prism and the rectangles make the lateral faces. We consider TG nanoprism with dimensions **w, h,** and **t**; **w** denotes the length of the base of the isosceles triangle, **h** denotes the length of a perpendicular line from the center of the tip to the middle of the base side, and **t** denotes the thickness of the nanoprism. To maximize coupling with the WGM microtoroid and also to maximize the observable intensity enhancement, we have assumed that the bases of the prism lie in the (y, z) plane such that its thickness lies in the x direction as in Fig. 2. Our calculations were performed for **TE** mode, thus making orientation of TG to be parallel to the mode polarization.

To indicate the size of the TG nanoprism which has localized plasmon resonances near the **TE** resonance of WGMR microtoroid (on-resonance), we provide a simulated scattering spectrum using MNPBEM toolbox,[32] which is a Matlab toolbox for the simulation of metallic nanoparticles (MNP) and solves the Maxwell's equations based on a boundary element method (BEM).[33,34] For most plasmonics applications with sizes ranging from a few nanometer to a few hundred nanometers, and for frequencies in the optical and near-infrared regime, BEM approach appears to be a natural choice. Fig. 3, shows scattering spectra of TG nanoprism with **h** = 24 nm, **w** = 120 nm, and **t** = 10 nm. As can be

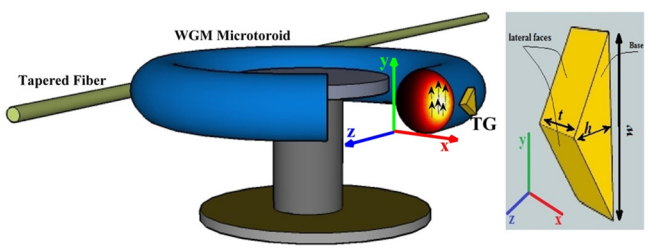

FIG. 2. Geometrical scheme of WGM microtoroid with a gold triangular nanoprism bound to its surface.

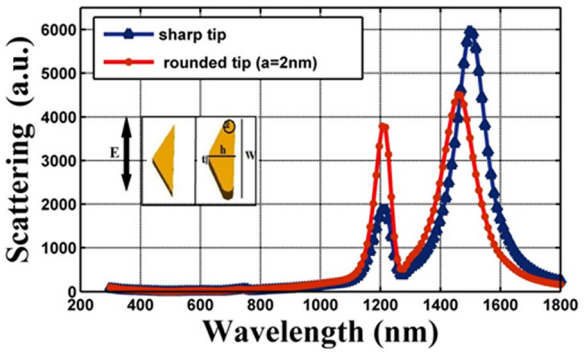

FIG. 3. Scattering spectra of gold triangular nanoprism for sharp tip and rounded tip (**a** = 2 nm) with **h** = 24 nm, **w** = 120 nm, **t** = 10 nm. The dielectric surrounding is modeled with an effective refraction index, $n = 1.33$. Gold refractive index is based on data from Palik.[31]

clearly seen from Fig. 3 for the triangular gold with sharp tips, the main resonance locates at $\lambda = 1498$ nm, together with one weak resonances at $\lambda = 1206$ nm. As the **TE** mode occurs at 1499.9 nm, the above mentioned nanoparticle dimensions chosen are optimal. It should be emphasized here that rounding the corners indeed reflects the practical feasibility of synthesis, therefore we introduce the radius of curvature **a** at the tip as a parameter, and we performe the simulation with round corners of radius of curvature of 2 nm which still has a very good degree of sharpness, but practically feasible. Moreover, despite that rounding the corners would lead to lower intensity enhancement, but it would provide to higher spatial extent making better area for analytic particles. For the triangular gold with radius of curvature of **a** = 2 nm, the main resonance is located at $\lambda = 1458$ nm and a weak resonance at $\lambda = 1204$ nm.

The distance between WGMR and TG is usually chosen such that the evanescent field would still possess its highest value before its decay. As shown in Fig. 4, when TG nanoprism was placed at a fixed distance of 5 nm from the microtoroid surface, we have maximum enhancement factor. According to our calculations, this field value is the best one chosen, since working with distances of 10 nm, 20 nm, and so on shows the very diminished value of LFIEF. In our simulation, distances less than 5 nm are not possible because of meshing problem.

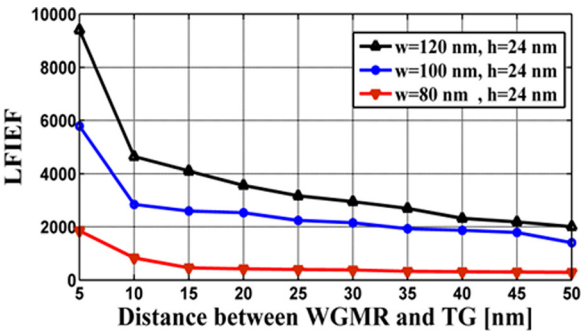

FIG. 4. LFIFE of TG nanoprism for different distances between WGMR and TG nanoprism (from 5 nm to 50 nm). The TG nanoprism has dimensions **w** = 80 nm, 100 nm, and 120 nm and **t** = 10 nm. The refractive index of dielectric surrounding is $n = 1.33$.

The LFIEF at corners in the case of TG nanoprism with $\mathbf{h} = 24\,\text{nm}$, $\mathbf{w} = 120\,\text{nm}$, and $\mathbf{t} = 10\,\text{nm}$ was enhanced by $\times 9400$ which is equivalent to 97 times enhancement in the field magnitude as seen in Fig. 5; this intense electric field results in a considerable resonance shift according to RSP and thereby improves sensitivity of the sensor.

We also quantitatively evaluate the quality factor, when using FEM with complex material permittivity and PMLs, the eigenfrequencies (f) are complex, where its real parts (f_{Re}) representing resonant frequencies and the imaginary parts (f_{Im}) representing the total intrinsic losses. Therefore, the Q-factor is defined as $Q = f_{\text{Re}}/2f_{\text{Im}}$.[35] In calculating the Q-factor of the complete coupled structure (microtoroid+TG), it should be noted that when we simulate a sector with a single nanoparticle, we are actually modeling a periodic array of nanoparticles around the resonator. Any change in the linewidth is hence due to N particles, where N is related to the angular width of our simulation sector. Assuming the width of our angular simulation volume is large enough so as to avoid coupling the nanoparticles, then the total broadening will be N times that of a single particle, i.e., the effects are additive. In this way, we can then get the contribution of a single particle to linewidth change from our simulated result by a simple division by N. While the plasmonic TG can significantly enhance the local field in its vicinity, it also absorbs and scatters light, thereby reducing the resonator enhancement by significant degradation of the cavity Q-factor from 4×10^7 (quality factors in the absence of the TG) to 7.6×10^3 (quality factors in the presence of the TG). We have also investigated cases far from a plasmonic resonances (off-resonance) that provide comparable performance,[29] for example, for $\mathbf{w} = 100\,\text{nm}$, $\mathbf{h} = 24\,\text{nm}$, and $\mathbf{t} = 10\,\text{nm}$, plasmon resonance of TG nanoprism lies at wavelengths of 1216 nm (main resonance) and 1307 nm (weak resonance), while the **TE** mode occurs at wavelength of 1499.9 nm. Therefore for this case, the resonance properties of the TG nanoprism are negligible, the LFIEF at corners enhanced by $\times 5500$ (by degrading the cavity Q-factor to 1.1×10^4) therefore the LFIEF (Q-factor) is lower (higher) than that of on-resonance case. Two key parameters for improving the sensitivity of a WGM hybrid biosensor are the resonance frequency shift (that is proportional to the LFIEF) and the quality factor. Figs. 6(a)–6(c) can be used to select a suitable sensor design. Increasing sharpness of the corners (with increasing **w** or decreasing **h**) leads to a strong field enhancement of the light intensity. As shown in Fig. 6(c), the TG nanoprism with dimensions $\mathbf{w} = 80$, $\mathbf{h} = 24$, $\mathbf{t} = 10\,\text{nm}$ has largest LFIEF $\times$ Q but for this case, LFIEF and therefore resonance frequency shift is not sufficiently large.

Also, the effect of rounded tip on the electric field enhancement is calculated. As shown in Fig. 7, in the case of the triangular shape with different edge roundings, the LFIEF at corners is enhanced by $\times 4880$ for $\mathbf{a} = 2\,\text{nm}$ (degradation of the cavity Q-factor to 4.3×10^4) and $\times 1860$ for $\mathbf{a} = 6\,\text{nm}$ (degradation of the cavity Q-factor to 1.27×10^5).

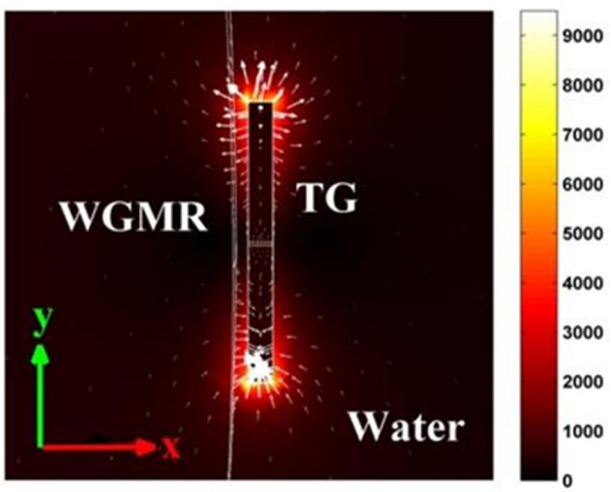

FIG. 5. LFIFE of TG nanoprism with dimensions of ($\mathbf{h} = 24\,\text{nm}$, $\mathbf{w} = 120\,\text{nm}$, $\mathbf{t} = 10\,\text{nm}$) for **TE** polarization of microtoroid-nanoprism system in (x, y) plane.

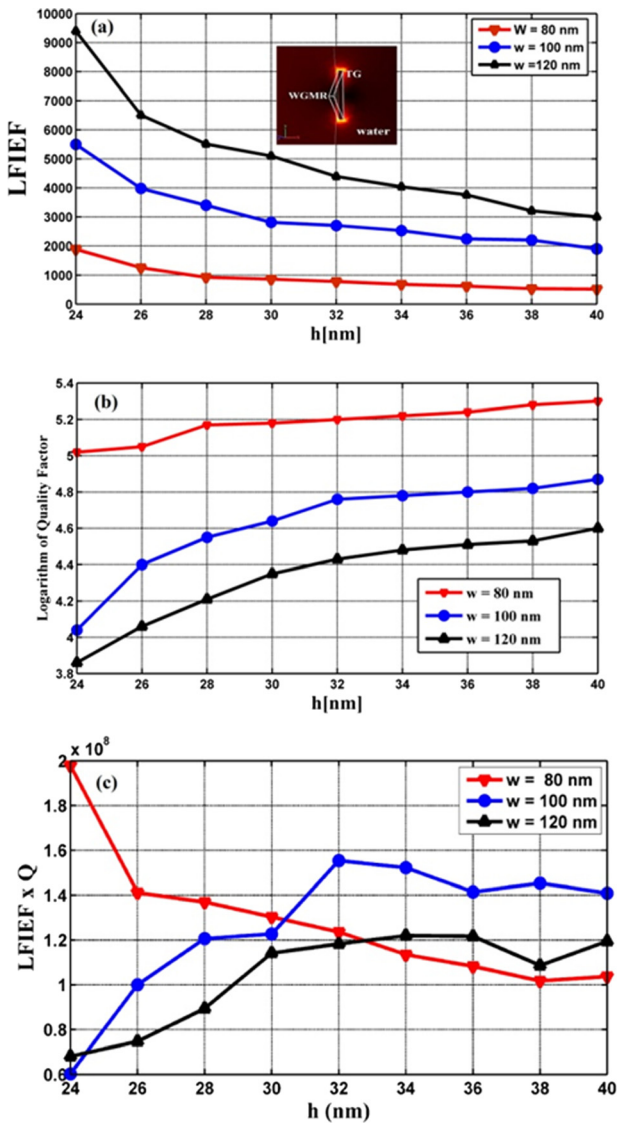

FIG. 6. (a) LFIFE of TG nanoprism for different **h** (from $\mathbf{h} = 24\,\text{nm}$ to $\mathbf{h} = 40\,\text{nm}$). (b) Quality factors on a logarithmic scale, i.e., $\log_{10}(Q)$. (c) LFIEF $\times$ Q, this product determines the sensor sensitivity. The TG nanoprism has dimensions $\mathbf{w} = 80\,\text{nm}$, 100 nm, and 120 nm, $\mathbf{t} = 10\,\text{nm}$ and TG nanoprism was placed at a fixed distance of 5 nm from the microtoroid surface. The refractive index of dielectric surrounding is $n = 1.33$.

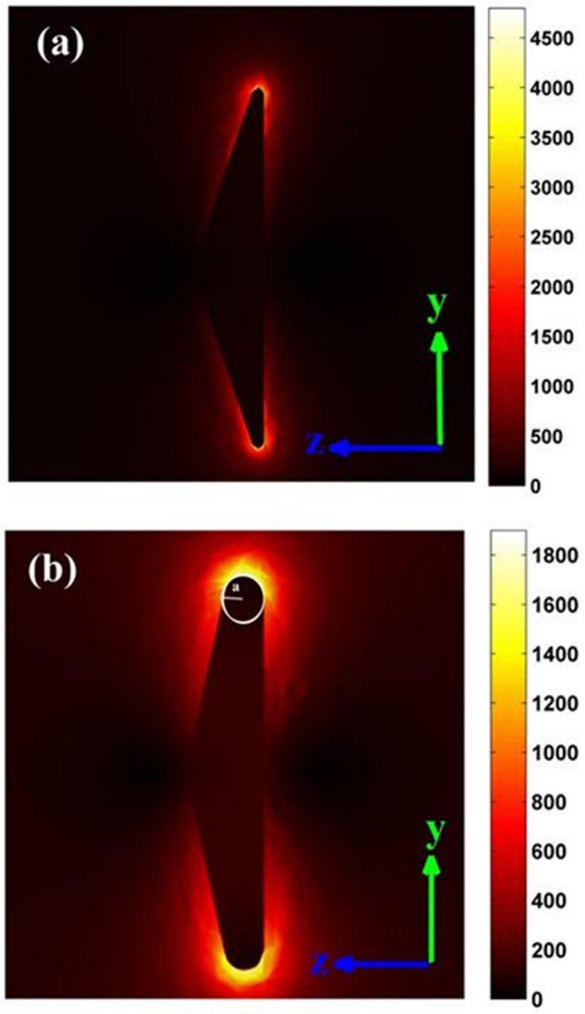

FIG. 7. LFIFE of TG nanoprism for different radius of curvatures; $\mathbf{a} = 2$ nm (a) and $\mathbf{a} = 6$ nm (b) for **TE** polarization. The TG nanoprism has dimensions of $\mathbf{h} = 24$ nm, $\mathbf{w} = 120$ nm, and $\mathbf{t} = 10$ nm in (y, z) plane.

As the radius of curvature is small, the hot spots play an important role in the field intensity enhancement and we have larger LFIEF and lower Q-factor. There is strong field intensity stored in the plasmon nanoprism resulting in two hot spots for **TE** mode.

Using RSP formula, Eq. (1), we would calculate the change in the resonance wavelength resulting from a single bovine serum albumin (BSA $\alpha_m = 54\,800$ Å^3)[36] proteins binding to a TG nanoprism. We can model the BSA molecule as a dielectric sphere with a radius of 3.4 nm. Using the polarizability for BSA from Ref. 36 and a radius of 3.4 nm, we use the standard formula for polarizability[37] to obtain a relative permittivity of 2.42 for BSA. We assume that the BSA molecule is attached to the upper pole of the plasmonic TG nanoprism, where the maximum field enhancement occurs in the **TE** mode. Fig. 8 shows the results of one of the calculations. The simulation has been performed with round corners of radius of curvature of $\mathbf{a} = 4$ nm which has a very good degree of sharpness, practically feasible, and comparable in size of BSA ($\mathbf{r} = 3.4$ nm). There is substantial overlap among the electric field and the dielectric of the protein molecule. For these simulations, the side length of the nanoprism

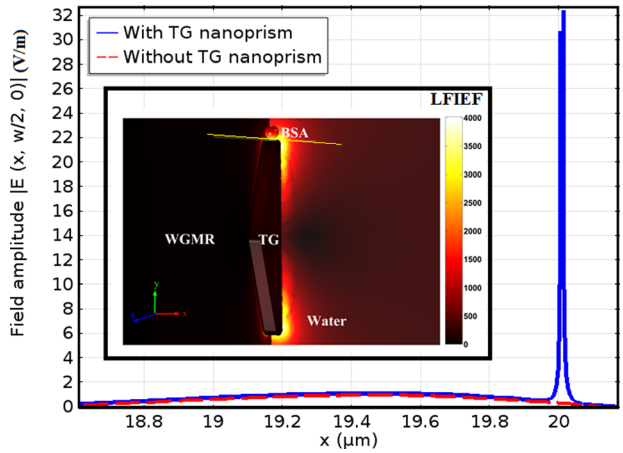

FIG. 8. Field amplitude of **TE** whispering gallery mode without TG nanoprism (dashed) and with TG nanoprism (solid) for a microtoroid with a major diameter of 36 μm and minor diameter of 4 μm. Line profiles were taken along the yellow line shown in inset. Inset shows LFIEF of a hybrid WGMR-TG nanoprism with radius of curvature $\mathbf{a} = 4$ nm, $\mathbf{h} = 24$ nm, $\mathbf{w} = 100$ nm, and $\mathbf{t} = 7$ nm and a single BSA is attached to the upper pole of the plasmonic TG.

was kept constant at $\mathbf{w} = 100$ nm and $\mathbf{t} = 7$ nm. It is worth mentioning here that field normalization plays a key role in the calculation of the field enhancement. As shown in Fig. 8, the field amplitude in the presence of the TG nanoprism is ~ 32 V/m, as compared to the amplitude at the same position without the TG nanoprism of ~ 0.5 V/m, the LFIEF is ~ 4090. Since the tip radius of TG nanoprism and the BSA protein are comparable in size (~ 4 nm), there is a effective overlap of the near field intensity and the dielectric volume as shown in Fig. 9. The simulations were carried out on four nanoprisms of different thicknesses corresponding to aspect ratios of 14.3 (100:7), 10 (100:10), 8.3 (100:12), and 6.6 (100:15), In these cases, a resonance shift of $\delta = 26.45$ fm, 19.87 fm, 13.78 fm, and 10.42 fm was noticed, respectively. These are a significant enhancement compared to a bare microtoroid, which has a shift of $\delta = 0.018$ fm. We computed the enhancement ratio (ξ) for the shift in the resonance wavelength, which examines the ratio of the shift in the WGMR in the presence of the TG nanoprism to that of the resonance shift without a TG nanoprism (i.e., the BSA protein alone attached to the bare microtoroid)

$$\xi = \frac{\boldsymbol{\delta\lambda}_{with\,TG}}{\boldsymbol{\delta\lambda}_{without\,TG}}.$$

Table I summarizes the results of the expected shifts in the resonance wavelength, the enhancement ratio ξ, and the Q-factor for adsorption of the BSA protein onto a hybrid WGMR-TG nanoprism.

IV. CONCLUSION

A label-free WGM biosensor coupled to plasmonic TG nanoprism was studied in this work. It is shown that the locally electric field enhancement usually required for optical sensing can well be promising for sensing purposes. Similar to nanoshells and nanorods, TG nanoprisms can

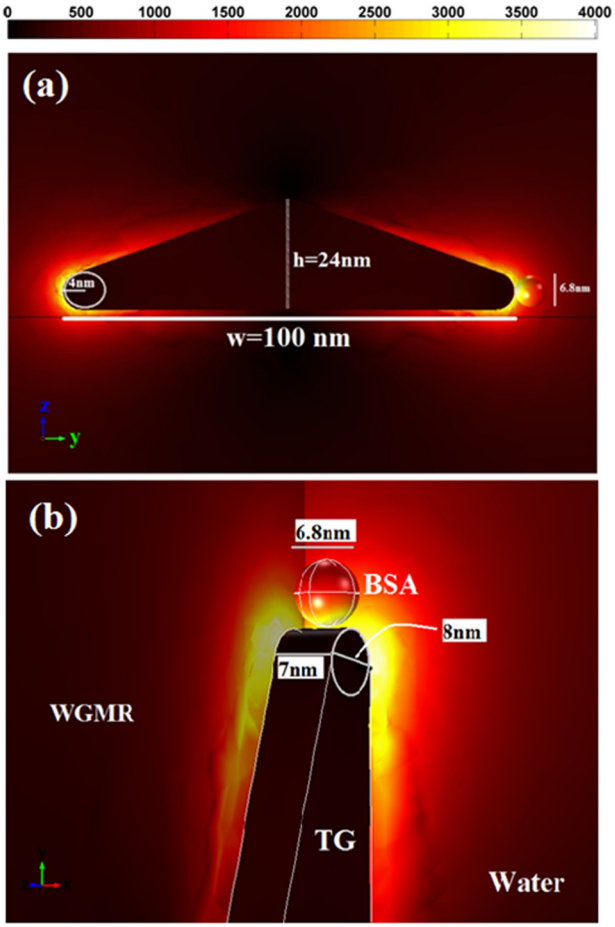

FIG. 9. (a) Image of the LFIEF obtained from FEM simulation of a spherical shaped BSA molecule situated top on a TG nanoprism with $\mathbf{a} = 4$ nm, $\mathbf{h} = 24$ nm, $\mathbf{w} = 100$ nm, and $\mathbf{t} = 7$ nm. The maximum LFIEF was computed to be ~4090. (b) Because the tip diameter and the thickness of TG nanoprism are comparable in diameter of BSA protein (~7 nm), there is effective overlap of the near field intensity at the dielectric volume.

afford the opportunity for tuning the localized plasmon resonance frequency by variation of the tip sharpness, the edge length, and the aspect ratio. Additionally, TG nanoprisms also exhibit much stronger near field enhancements than nanoshells and nanorods due to its sharper geometrical features, hence motivating their use in sensing applications.

The tips of the nanoprisms are associated with the greatest plasmonic electric field enhancement known as hot-spots. The effect of rounded tips on the electric field enhancement is also studied. Calculation showed that although in the case of sharp tips, one can have better field enhancement, but reduction in Q-factor will be experienced such that this low Q-factor configuration can no longer be suitable for ultrasensitive sensing purposes. Moreover for the case of sharp tip, the hot spots play an important role in the field intensity enhancement and where we have larger LFIEF and lower Q-factor. The results of this work thereby can make the detection and characterization of some large protein molecules possible. We have successfully demonstrated the detection of single BSA proteins using our hybrid microcavity. When the tip diameter and the thickness of TG nanoprism are comparable in diameter of BSA protein (~7 nm), there is effective overlap of the near field intensity at the dielectric volume. We have shown that the resonance wavelength shift $\delta = 26.45$ fm is caused by binding a single BSA protein to the TG nanoprism with tip radius $\mathbf{a} = 4$ nm and thickness $\mathbf{t} = 7$ nm, the enhancement was found to be $\xi \sim 1469$ and degradation of the cavity Q-factor was found to be 3.6×10^4.

TABLE I. Summary of the expected wavelength resonance shifts, the enhancement ratio ξ, and the Q-factor for a single bovine serum albumin protein adsorbed onto a TG nanoprism with different AR.

AR	14.3	10	8.3	6.6	Bare microtoroid
$\delta\lambda$	26.45 fm	19.87 fm	13.78 fm	10.42 fm	0.018 fm
ξ	1469	1103	765	578	—
Q-factor	3.6×10^4	6.1×10^4	8.7×10^4	1.13×10^5	4×10^7

[1]B. M. Willardson, J. F. Wilkins, T. A. Rand, J. M. Schupp, K. K. Hill, P. Keim, and P. J. Jackson, Appl. Environ. Microbiol. **64**(3), 1006 (1998).
[2]J. Tschmelak, G. Proll, and G. Gauglitz, Anal. Chim. Acta **519**(2), 143 (2004).
[3]A. J. Baeumner, R. N. Cohen, V. Miksic, and J. Min, Biosens. Bioelectron. **18**, 405 (2003).
[4]Y. M. Bae, B. K. Oh, W. Lee, W. H. Lee, and J. W. Choi, Biosens. Bioelectron. **20**(4), 895 (2004).
[5]M. Baaske and F. Vollmer, ChemPhysChem **13**, 427 (2012).
[6]T. Yoshie, L. L. Tang, and S. Y. Su, Sensors **11**, 1972 (2011).
[7]A. Chiasera, Y. Dumeige, P. Feron, M. Ferrari, Y. Jestin, G. N. Conti, S. Pelli, S. Soria, and G. C. Righini, Laser Photonics Rev. **4**, 457 (2010).
[8]F. Vollmer and S. Arnold, Nat. Methods **5**, 591 (2008).
[9]F. Vollmer, S. Arnold, and D. Keng, Proc. Natl. Acad. Sci. U.S.A. **105**(52), 20701 (2008).
[10]S. Arnold, M. Khoshsima, I. Teraoka, S. Holler, and F. Vollmer, Opt. Lett. **28**(4), 272 (2003).
[11]Y. Hu, L. Shao, S. Arnold, Y.-C. Liu, C.-Y. Ma, and Y.-F. Xiao, Phys. Rev. A **90**, 043847 (2014).
[12]I. Teraoka and S. Arnold, J. Opt. Soc. Am. B **23**, 1381 (2006).
[13]J. T. Rubin and L. Deych, Phys. Rev. A **81**, 053827 (2010).
[14]Y.-F. Xiao, Y.-C. Liu, B.-B. Li, Y.-L. Chen, Y. Li, and Q. Gong, Phys. Rev. A **85**, 031805 (2012).
[15]M. R. Foreman and F. Vollmer, New J. Phys **15**, 083006 (2013).
[16]S. I. Shopova, R. Rajmangal, S. Holler, and S. Arnold, Appl. Phys. Lett. **98**, 243104 (2011).
[17]V. R. Dantham, S. Holler, V. Kolchenko, Z. Wan, and S. Arnold, Appl. Phys. Lett. **101**(4), 043704 (2012).
[18]V. R. Dantham, S. Holler, C. Barbre, D. Keng, V. Kolchenko, and S. Arnold, Nano Lett. **13**(7), 3347 (2013).
[19]J. D. Swaim, J. Knittel, and W. P. Bowen, Appl. Phys. Lett. **99**, 243109 (2011).
[20]P. Zijlstra, P. M. R. Paulo, and M. Orrit, Nat. Nanotechnol. **7**, 379 (2012).
[21]S. Arnold, V. R. Dantham, C. Barbre, B. A. Garetz, and X. D. Fan, Opt. Express **20**(24), 26147 (2012).
[22]M. D. Baaske, M. R. Foreman, and F. Vollmer, Nat. Nanotechnol. **9**, 933–939 (2014).
[23]A. Singh, M. Chaudhari, and M. Sastry, Nanotechnology **17**, 2399 (2006).
[24]H. Jing, L. Zhang, and H. Wang, *Geometrically Tunable Optical Properties of Metal Nanoparticles* (Springer-Verlag, Berlin, Heidelberg, 2013).
[25]E. C. Le Ru and P. G. Etchegoin, *Principles of Surface-Enhanced Raman Spectroscopy and Related Plasmonic Effects* (Elsevier, Amsterdam, 2009).
[26]D. K. Armani, T. J. Kippenberg, S. M. Spillane, and K. J. Vahala, Nature **421**, 925 (2003).
[27]A. B. Matsko and V. S. Ilchenko, IEEE J. Sel. Top. Quantum Electron. **12**, 3–14 (2006).
[28]M. Oxborrow, IEEE Trans. Microwave Theory Tech. **55**, 1209 (2007).
[29]A. Kaplan, M. Tomes, T. Carmon, M. Kozlov, O. Cohen, G. Bartal, and H. G. L. Schwefel, Opt. Express **21**, 14169 (2013).
[30]X. Du, S. Vincent, and T. Lu, Opt. Express **21**(19), 22012 (2013).

[31]E. D. Palik, *Handbook of Optical Constants of Solids* (Academic Press, Boston, 1985).
[32]U. Hohenester and A. Trügler, Comput. Phys. Commun. **183**, 370 (2012).
[33]F. J. Garcia de Abajo and A. Howie, Phys. Rev. B **65**, 115418 (2002).
[34]F. J. G. de Abajo, Rev. Mod. Phys. **82**, 209 (2010).
[35]D. M. Pozar, *Microwave Engineering* (Wiley, 1998).
[36]F. Vollmer, B. I. F. Futura **20**, 239 (2005).
[37]J. Jackson, *Classical Electrodynamics* (Wiley, New York, 1999).